NANO LETTERS

Letter

pubs.acs.org/NanoLett

Aluminum Nanoantenna Complexes for Strong Coupling between Excitons and Localized Surface Plasmons

Elad Eizner,* Ori Avayu, Ran Ditcovski, and Tal Ellenbogen

Department of Physical Electronics, Fleischman Faculty of Engineering, Tel Aviv University, Tel Aviv 69978, Israel

Supporting Information

ABSTRACT: We study the optical dynamics in complexes of aluminum nanoantennas coated with molecular J-aggregates and find that they provide an excellent platform for the formation of hybrid exciton-localized surface plasmons. Giant Rabi splitting of 0.4 eV, which corresponds to ~10 fs energy transfer cycle, is observed in spectral transmittance. We show that the nanoantennas can be used to manipulate the polarization of hybrid states and to confine their mode volumes. In addition, we observe enhancement of the photoluminescence due to enhanced absorption and increase in the local density of states at the exciton-localized surface plasmon energies. With recent emerging technological applications based on strongly coupled light−matter states, this study opens new possibilities to explore and utilize the unique properties of hybrid states over all of the visible region down to ultraviolet frequencies in nanoscale, technologically compatible, integrated platforms based on aluminum.

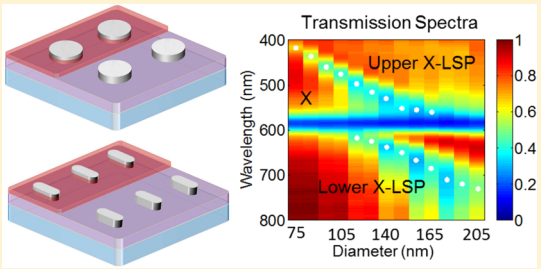

KEYWORDS: *Strong coupling, aluminum nanoantennas, organic polaritons, localized surface plasmons*

The interaction between light and quantum emitters such as excitons depends on the local density of electromagnetic (EM) modes. Increasing the density of EM modes, e.g., by using optical cavities, can facilitate faster energy transfer between the electronic material-excitations and the EM fields, leading to a variety of interesting physical phenomena such as the Purcell enhancement[1] where the lifetime of excited states is reduced leading to brighter light emission. When the rate of energy exchange between the excitons and the local EM modes becomes higher than their individual rates of decay and decoherence, hybrid light−exciton states emerge with new and exciting mixed properties of light and matter.[2,3] Unlike photons, these hybrid light−matter states can collide and scatter through polariton−polariton and polariton−exciton interactions.[4] Therefore, hybridization leads to population-dependent nonlinearities which can result in polariton condensation and macroscopic coherence of the hybrid states and of the emitted light.[2] As a result, novel applications based on hybrid states are emerging, such as the generation of low threshold coherent emission at room temperature without the need for population inversion,[5,6] parametric amplification of optical signals,[7] and ultrafast switching.[8,9] In addition, as was recently demonstrated, strong coupling with EM modes can even modify energy transfer pathways, e.g., within organic molecules[10] and photosynthetic organisms,[11,12] and can be used to develop nanoscale quantum devices.[13] In light of all of these potential applications, the technological compatibility of the platform in which the hybrid states are generated is extremely important.

A wide variety of platforms including optical microcavities,[2,4−6,14−16] optical waveguides,[17−21] optical lattices,[22,23] flat metal surfaces,[24−28] and metallic nanoparticles[29−35] have already been used to demonstrate strong coupling between EM fields and excitons. Of these, the metallic nanoparticle platform carries several advantages. First of all, the EM fields associated with the localized surface plasmon (LSP) modes of the metallic nanoparticles are confined to deep subwavelength volumes in all three dimensions. This confinement provides a way to focus light in the nanoscale which enhances the coupling with excitons and reduces the footprint of the active area. In addition, the optical response of the metallic nanoparticles, e.g., their resonance frequency and polarization, can be easily controlled by adjusting the shape, size, and chemical composition of the particles. This enables control of the effective optical properties of the bulk materials and the construction of so-called metamaterials.[36−41] Overall metal nanoparticles permit customization of EM interaction with the excitons to attain strong coupling in an easily integrated and ultracompact platform.

In recent years several groups have studied strong coupling between excitons and LSPs in metallic particles made from gold[33−35] or silver.[29−32] Gold is considered a good and stable plasmonic material; however, it is limited to work at energies below 2.4 eV where the onset of s−d interband transitions damps the LSPs. The first interband transitions in silver occur at higher energies (~3.1 eV); however, it reacts quickly with oxides and sulfides which degrade the purity over time. Therefore, in order to improve the technological compatibility, additional materials should be investigated.

Received: June 30, 2015
Revised: August 6, 2015
Published: August 10, 2015

DOI: 10.1021/acs.nanolett.5b02584
Nano Lett. 2015, 15, 6215−6221

Very recently, aluminum (Al) was shown to be an outstanding material for nanoplasmonic based systems.[42−47] Aluminum has an interband transition at a narrow energy band around 1.5 eV, and therefore Al nanoparticles can support LSPs with relatively long lifetimes and large optical cross sections[42−44] over a wide energy range, comprising the visible region down to ultraviolet frequencies. Furthermore, Al is cheap, abundant (the most abundant metal in the Earth's crust), and forms a 2−3 nm stable oxide (Al_2O_3) layer almost immediately on exposure to air. This layer protects and preserve the nanoparticles, giving them long-term durability.[42] Aluminum is therefore a very attractive candidate for technological device applications, and it is interesting to examine its compatibility for generating hybrid exciton−plasmon states. Currently there is no reported evidence for strong coupling between excitons and bright (dipolar) LSP modes in Al nanoparticles. The only reported observation was between excitons in ZnO quantum wells coupled to plasmonic quadrupole modes in Al nanoparticles, and these exhibited only a relatively small Rabi energy splitting of 0.015 eV.[48] In that case, the possible applications are limited due to the dark nature of the plasmon modes and the close to dissipation rate value of the Rabi splitting. Here we demonstrate that complexes of Al nanoantennas coated with J-aggregating molecules can be used for efficient generation of bright hybrid exciton-LSP states (X-LSPs). We use spectral transmittance to measure a giant, 0.4 eV, energy dispersion Rabi splitting as a consequence of the formation of hybrid states and find that the nanoantennas can also be used to control their polarization. In addition we observe enhancement of the light emission from the J-aggregate−Al nanoantennas in specific spectral regions corresponding to the hybrid X-LSP modes.

Theoretical Framework. The interaction between N two-level systems and photons of an EM mode can be described by the Dicke model.[49] At the limit where N is large compared to the number of photons in the system, the collection of two level systems acts like a giant quantum oscillator, and the coupling energy is $g \propto N^{1/2}\vec{\mu}\vec{E}$.[3,50] For a system of excitons interacting with LSPs, $\vec{\mu}$ is the excitonic transition dipole moment, and $\vec{E}$ is the electric field component of the LSP at the transition energy. For a homogeneous layer of excitonic transition dipoles (TDs), the number of TDs that interact with an LSP mode is $N = n_X V_X$, where n_X is the density of the TDs and V_X is the result of the overlap integral between the LSP mode and the distribution of TDs. The coupling energy therefore takes the form

$$g = F\mu\sqrt{\frac{n_X U_X}{\epsilon_0 \epsilon_d}}\sqrt{\frac{V_X}{V}} \tag{1}$$

where U_X is the transition energy, V is the effective LSP mode volume, quantifying the electric field strength per LSP, F is a factor that depends on the orientation of the dipoles, ϵ_0 is the vacuum permittivity, and ϵ_d is the dielectric constant outside the nanoparticle. From eq 1, it can be seen that due to the collective nature of the interaction, one of the main quantities that affects the coupling strength is the ratio between the overlap volume V_X and the total mode volume V. Reduction of the EM mode volume is usually recommended to increase light−matter interactions. However, from eq 1, it can be seen that for homogeneously spread TDs, reducing the mode volume also correspondingly reduces the number of interacting TDs within the mode ($n_X V_X$), and as a consequence the coupling strength does not increase. This can be seen as one of the signatures of collective strong coupling with many TDs. By geometrical manipulations of nanoantennas, the mode volume can be confined and reduced. However, it is important to understand that this would not necessarily increase the coupling strength.

Many features of X-LSPs and strong coupling physics can be understood in terms of coupled harmonic oscillators.[2,3,51] Adopting this model:

$$\begin{pmatrix} U_{LSP} - i\frac{\gamma_{LSP}}{2} & g \\ g & U_X - i\frac{\gamma_X}{2} \end{pmatrix}\begin{pmatrix}\alpha \\ \beta\end{pmatrix} = U_{LP,UP}\begin{pmatrix}\alpha \\ \beta\end{pmatrix} \tag{2}$$

where U_{LSP}, U_X and γ_{LSP}, γ_X are the uncoupled LSP and exciton energies and decay rates respectively, $U_{LP,UP}$ are the energies of the hybrid states, and α and β are the weighting coefficients of the LSPs and excitons in the hybrid states, where $|\alpha|^2 + |\beta|^2 = 1$. The eigenvalues of eq 2 which describe the energies of the hybrid modes are

$$U_{LP,UP} = \frac{1}{2}\left[U_X + U_{LSP} - i\left(\frac{\gamma_X}{2} + \frac{\gamma_{LSP}}{2}\right) \pm \sqrt{4g^2 + \left(U_X - U_{LSP} - i\left(\frac{\gamma_X}{2} - \frac{\gamma_{LSP}}{2}\right)\right)^2}\right] \tag{3}$$

Therefore, considering a nondispersive exciton and size-dispersive LSP, the signature of the coupled system shows a split of the dispersion relation corresponding with the upper and lower exciton polaritons. To observe Rabi splitting, the difference between the upper and lower energies of the polaritons, $(4g^2 - ((\gamma_X/2) - (\gamma_{LSP}/2))^2)^{1/2}$, should be larger than the polariton line width $(\gamma_X/2) + (\gamma_{LSP}/2)$, resulting in the following condition for strong coupling and Rabi splitting:[3,52,53]

$$\hbar\Omega_R = 2g > \sqrt{\frac{\gamma_X^2}{2} + \frac{\gamma_{LSP}^2}{2}} \tag{4}$$

It is important to note that, even with coupling energies that do not fulfill the condition in eq 4, the interaction between the LSP and exciton modes can result in spectral splitting and asymmetric line shapes (e.g., Fano resonances),[52,54] although these do not indicate Rabi energy transfer. This is an important point with respect to aluminum plasmonics, which can suffer from faster damping rates of the LSP modes compared to noble metals.

The interaction between LSPs and excitons can be studied either by using single nanoantennas[32,34,35] or by using arrays of subwavelength spaced nanoantennas.[29] If the nanoparticle size is smaller than the separation distance between the closest neighbors, near field interparticle coupling can be neglected,[55] and the resonances in each array are determined by the LSP resonances of individual nanoparticles.

Experiment and Results. The studied samples, as illustrated in Figure 1, consisted of subwavelength-spaced arrays of Al nanodisks and nanorods fabricated on indium tin oxide (ITO) coated glass substrate and covered with a thin (∼20 nm) layer of J-aggregating cyanine dye molecules (TDBC). All of the nanoantennas were 40 nm thick, and the area of each of the arrays was 15 × 15 μm^2. As illustrated in Figure 1a, each nanodisk array had a different disk diameter, D, ranging from 75 nm to 205 nm, and a fixed side to side

DOI: 10.1021/acs.nanolett.5b02584
Nano Lett. 2015, 15, 6215−6221

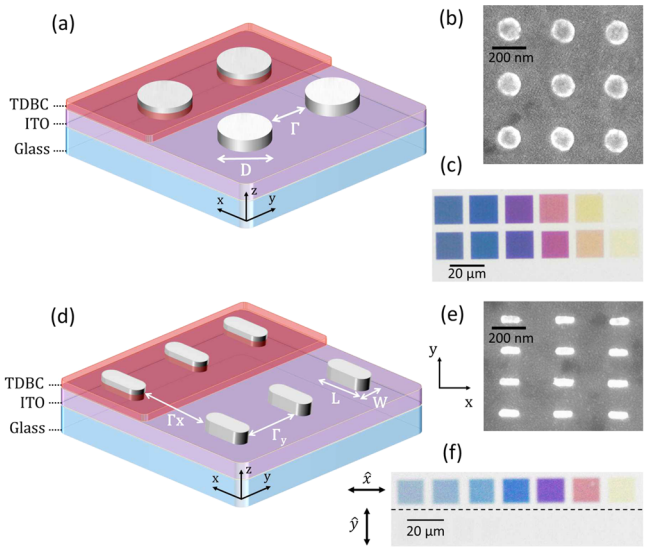

Figure 1. Aluminum nanoantenna based X-LSP samples. (a) Illustration of nanodisk based X-LSP samples (b) SEM image of a sample of nanodisks with D = 140 nm and Γ = 180 nm. (c) White light transmission image through bare nanodisk arrays with different diameters. (d) Illustration of nanorod based X-LSP samples (e) SEM image of a sample of nanorods with L = 120 nm, W = 40 nm, Γ_y = 150 nm, and Γ_x = 200 nm. (f) Polarized white light transmission image for an incident light polarized at the x (top part) or y (bottom part) axis, through bare nanorod arrays with different lengths. For light polarized along the y axis the sample becomes transparent in the visible region.

separation, Γ, which was ~180 nm. Each nanorod array (Figure 1d), had a different rod length, L, ranging from 75 nm to 205 nm, with a fixed side to side separation in the x direction, Γ_x, and in the y direction, Γ_y, (~200 nm and ~150 nm, respectively). A scanning electron microscope (SEM) image of one of the bare nanodisk arrays (D = 140 nm) is shown in Figure 1b, and an image of white light transmission through 12 arrays with different nanodisk diameters is shown in Figure 1c. The vivid colors in the transmission image are due to size dependent resonant coupling of the light to the dipolar LSPs of the nanodisks, which scatter and absorb the light at the LSP resonance. A scanning electron microscope (SEM) image of one of the nanorod arrays (L = 120 nm) is shown in Figure 1e, and an image of polarized white light transmission through the nanorod arrays is shown in Figure 1f. In this case, coupling to LSPs becomes polarization dependent. When the polarization is along the long axis, vivid colors are observed due to coupling to LSPs across the entire visible spectrum. When the polarization is rotated by 90°, the sample becomes transparent due to coupling to ultraviolet LSPs.

We used TDBC J-aggregates as the excitonic material because of their remarkable optical properties including delocalization of the exciton, narrow absorption and emission spectra, high binding energy, and large oscillator strengths (order of 10 D),[56] which allow them to couple strongly to EM fields at room temperature. The absorption and fluorescence spectra of water-TDBC solution spin coated on ITO coated glass is shown in Figure 2a. The J-band absorption peak is at 2.1 eV and has a line width of ~0.066 eV. The fluorescence exhibits slightly narrower line width and a very small Stokes shift of ~0.007 eV.

The coupling between the LSP modes on the nanoantennas and the excitons in the J-aggregates occurs in the overlap region of the J-aggregates and the LSP modes. Figure 2b and c shows finite difference time domain (FDTD) simulations of the LSP electric field enhancement in the x–y plane for a nanodisk and a nanorod, respectively, which were tuned to support an LSP resonance at the same wavelength (λ = 530 nm). As can be seen, there is a significant difference between the size of the nanodisks and nanorods that support a given LSP resonance. The simulated size of the nanorods is about three times smaller than the nanodisks. This is also supported by experimental results shown in Figures 3a and 4a. For small nanoantennas, a large fraction of the mode energy is stored within the metal in the electron motion,[57,58] and the LSP mode volume scales with the nanoantenna size. As a consequence, the LSP mode volumes on nanorods are considerably smaller than those on nanodisks tuned to support the same resonance frequency. This might be considered beneficial for strong coupling. However, as discussed earlier, for the case of a homogeneous layer of excitonic dipoles, as the mode volume is reduced, the number of dipoles inside the mode volume is also decreased. This is in accordance with experimental observations as described below.

To examine the EM modes of the system we measured the spectral transmittance through the nanoparticle samples, with and without the layer of TDBC J-aggregating dyes (see Methods). Figure 3a shows the measured transmission through bare nanodisk arrays with varying disk diameters. The dips in the transmission spectra correspond to coupling to LSPs and the modification of the position of the spectral dip reflects the size-dependent dispersion of the LSPs. The samples were then coated with TDBC J-aggregating dyes and the spectral

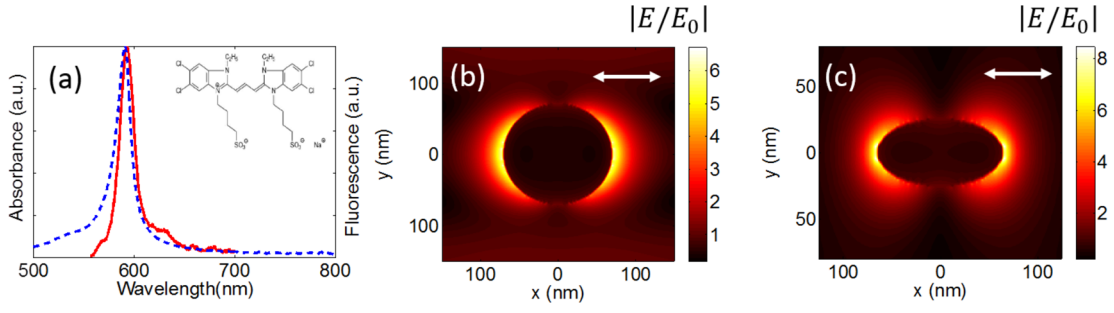

Figure 2. (a) Absorbance (blue dashed line) and fluorescence (red solid line) spectra of a thin TDBC layer on glass. The inset shows the chemical formula of TDBC. (b) FDTD simulations of electric field enhancement by nanodisks with diameter D = 140 nm and (c) nanorods, modeled as ellipses, with the major axis 65 nm long and the minor axis 25 nm long. Arrows mark the direction of the incident light polarization. The simulations were three-dimensional, periodic in the x–y plane, and the field monitors were placed 10 nm above the ITO layer (see Methods).

DOI: 10.1021/acs.nanolett.5b02584
Nano Lett. 2015, 15, 6215–6221

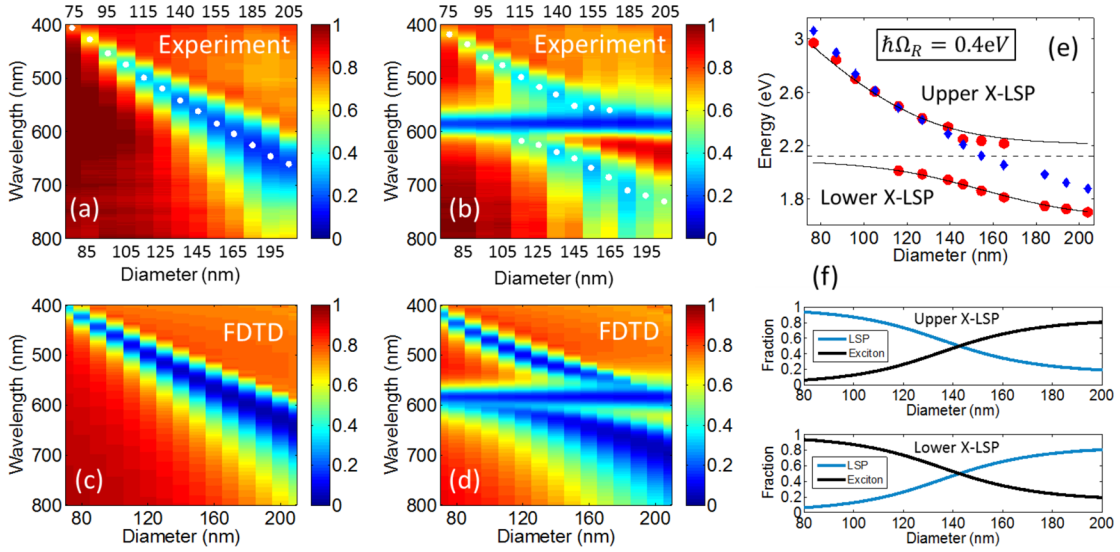

Figure 3. Transmission spectra of nanodisk arrays. (a) Normalized transmission spectra of bare nanodisk arrays. (b) Normalized transmission spectra of TDBC J-aggregates coated nanodisk arrays. (c) 3D FDTD normalized transmission spectra simulations of bare nanodisk arrays. (d) 3D FDTD normalized transmission spectra simulations of nanodisk arrays covered by a 20 nm layer of TDBC. (e) Energies of the transmission dips as a function of the diameter of the nanodisk array. Blue diamonds: bare nanodisk arrays. Red dots: nanodisk arrays coated with TDBC J-aggregates. Dashed line: bare TDBC J-aggregates layer absorption energy peak. Solid lines: theoretical fit using a coupled oscillator model. (f) Exciton and LSP fractions (calculated using a coupled oscillator model) of the upper or lower X-LSP polariton states.

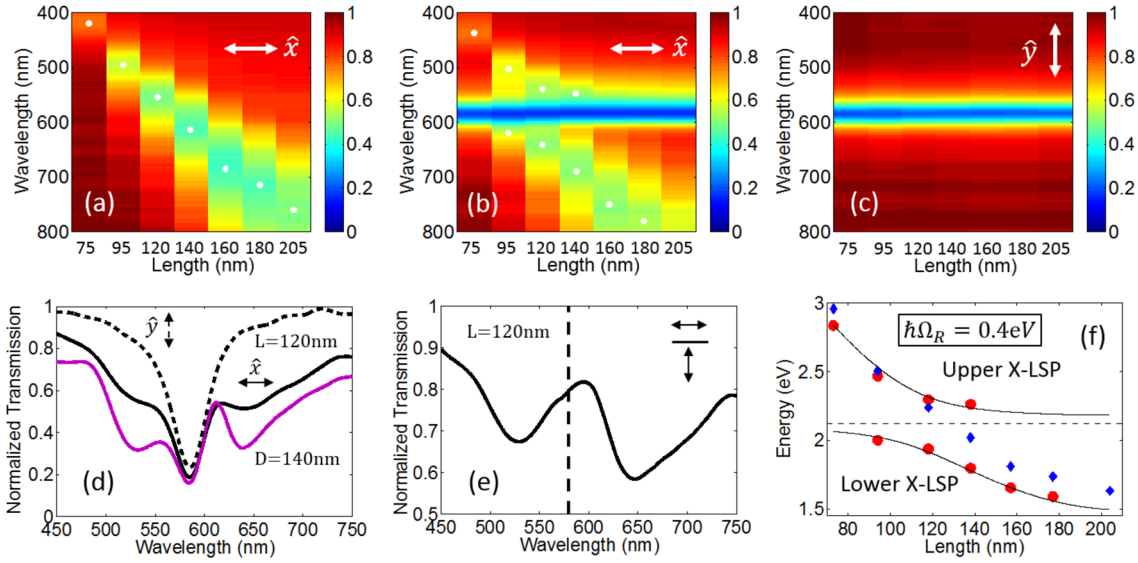

Figure 4. Transmission spectra of nanorod arrays. (a) Normalized transmission spectra of bare nanorod arrays with the incident light polarized along the long axis of the nanorods. (b) Normalized transmission spectra of TDBC J-aggregate dye coated nanorod arrays with the incident light polarized along the long axis of the nanorods and (c) with the light polarized along the short axis. (d) Normalized transmission spectra of an array of coated nanodisks with diameter D = 140 nm (purple solid line) and an array of coated nanorods with length L = 120 nm with the incident light polarized along either the long axis (black solid line) or the short axis (black dashed line) of the nanorods. (e) Transmission spectra of a coated array of nanorods with length L = 120 nm with the incident light polarized along the long axis of the nanorods, normalized to the transmission spectra of the same array with the incident light polarized along the short axis of the nanorods. The dashed line marks the TDBC J-aggregate absorption peak. (f) Energies of the transmission dips as a function of nanorod array length. Blue diamonds: bare nanorod arrays. Red dots: coated nanorod arrays. Solid lines were calculated from the coupled oscillator model (g = 0.2 eV and f = 0.95). Dashed line: Absorption peak of the TDBC J-aggregate layer.

transmittance was measured once again as shown in Figure 3b. In this case we can see several features in the transmission spectra. First, the appearance of a dispersionless dip at wavelength of 590 nm which corresponds to absorption due to uncoupled J-aggregate excitons. In addition there are two dispersive dip branches which correspond to the upper and lower polaritons of the coupled system. The splitting in the polariton branches is due to strong coupling between the excitons and LSP modes when the LSP energy is tuned across the exciton energy. When the LSP and exciton modes are largely detuned, the polaritons are indistinguishable from uncoupled LSP or exciton modes. These experimental results agree well with FDTD simulations as can be seen in Figure 3c and d (see Methods).

DOI: 10.1021/acs.nanolett.5b02584
Nano Lett. 2015, 15, 6215−6221

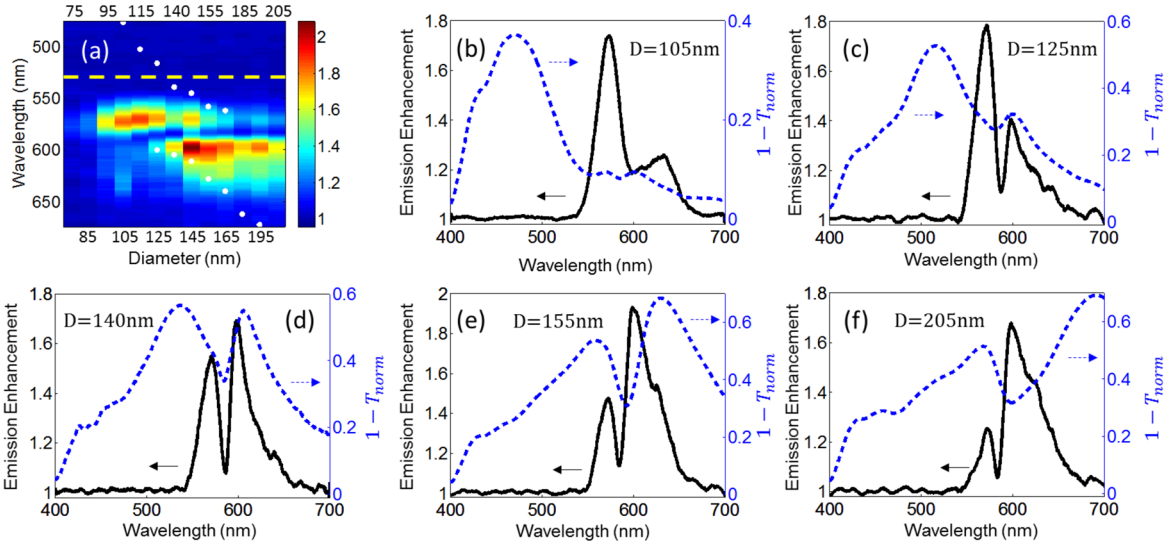

Figure 5. Emission enhancement. (a) Emission from TDBC J-aggregate coated nanodisk arrays, normalized to the emission from a TDBC J-aggregate layer (yellow dashed line marks the excitation wavelength: 530 nm). (b-f) Emission enhancement (solid black lines) and $1 - T_{norm}$ (dashed blue lines) as a function of wavelength for nanodisk arrays at 105 nm, 125 nm, 140 nm, 155 nm, and 205 nm, respectively. T_{norm} is the transmission spectra of coated arrays of nanodisks normalized to the transmission of a layer of TDBC J-aggregates.

The resonance energies as a function of nanodisk diameters are shown in Figure 3e. It is important to emphasize that the bare LSP measurements (blue diamonds) were performed before coating the sample with the layer of J-aggregating dyes. The coating also changes the background dielectric constant which redshifts the uncoupled LSP resonances. Taking this effect into account, the uncoupled LSP resonance for a diameter of 140 nm crosses the exciton resonance. The experimental results of polariton branches are compared to a coupled oscillator model by $U_{LP,UP} = 1/2\{U_X + fU_{LSP} \pm [4g^2 + (U_X - fU_{LSP})^2]^{1/2}\}$, where U_X and U_{LSP} are derived from the experimental transmission dips of the uncoupled systems. The fitting parameters include the coupling strength $g = 0.2$ eV and an additional parameter $f = 0.95$, which takes into account the change of bare LSP resonances due to the change in the background dielectric constant after coating the samples with the layer of J-aggregates. It can be seen that the experimental results are in excellent agreement with the model. Despite the oxide layer naturally formed on the Al nanoparticles, there is still a huge Rabi splitting of 0.4 eV in the energy dispersion, corresponding to an ultrafast periodic energy exchange between the excitons and LSP modes on a 10*fs* time scale.

The coupled oscillator model was also used to calculate the fractions of excitons and LSPs in the lower and upper polaritons as shown in Figure 3f. It can be seen that the polariton modes become half LSP and half exciton for an Al nanodisk with a diameter of ~140 nm.

For the nanorod samples we observe polarization effects of the hybrid modes. Figure 4a shows the measured polarized spectral transmittance with respect to the length of the bare Al nanorods. Figure 4b and c show the polarized spectral transmission through TDBC J-aggregate dye-coated nanorod arrays for an incident light polarized along the long or short axis of the nanorods, respectively. In Figure 4b, when the light is polarized along the long axis of the nanoantennas, we observe transmission dips that correspond to new upper and lower polariton branches. On the other hand, when the incident light is polarized along the short axis of the nanorods (Figure 4c) we observe a transmission dip only at the absorption of the uncoupled J-aggregate dyes. The transmission probes the modes of the coupled system as an average of more than 1500 nanorod antennas. In addition, from the measured splitting values and estimation of mode volume it can be calculated that the interaction region of each nanorod includes several thousands of participating J-aggregate excitons (see Supporting Information S3). Therefore, the hybrid X-LSPs are polarized due to the geometry of the nanoantennas, and the linear dichroism spectra does not fluctuate even at the level of a single nanorod. The experimental results agree with the FDTD simulations (see Supporting Figure S1). A comparison between the spectral transmissions through a coated array of nanorods with $L = 120$ nm and an array of nanodisks with $D = 140$ nm is shown in Figure 4d. It can be seen that, as described above, the splitting is comparable in the two cases despite the fact that the mode volume of the LSPs on the nanorods is smaller than that on the nanodisks. It can also be seen that the nanodisks scatter more strongly than the nanorods due to the different cross sections, leading to more pronounced spectral dips. Due to the fact that the hybrid states supported by the nanorods are polarized, the contribution of the uncoupled excitons to the transmission spectra can be removed simply by dividing the transmission at the two polarizations, as shown in Figure 4e. The resonance energies of the hybrid states as a function of nanorod lengths are shown in Figure 4f. As for the nanodisks, a giant splitting (0.4 eV) is observed in the energy dispersion of the nanorods. It is important to note that, although the nonradiative damping of aluminum is higher than that of gold or silver, the condition for strong coupling eq 4 is fully fulfilled for the nanodisk and nanorod arrays measured in this study.

We also studied the emission properties of the system (see Methods). Due to the large number of uncoupled excitons that contribute to the emission, we could not observe splitting in the direct emission from the sample. In order to extract the contribution of the hybrid X-LSP modes to the emission, we normalized the emission from TDBC J-aggregate coated nanodisk arrays to the emission from just the TDBC J-aggregates. Figure 5a shows the normalized spectral emission results obtained using a pulsed femtosecond laser excitation

DOI: 10.1021/acs.nanolett.5b02584
Nano Lett. 2015, 15, 6215−6221

with wavelength of 530 nm. An enhancement of the emission can be seen in specific spectral regions for each array. With respect to the exciton energy, the enhancement for shorter wavelengths is more pronounced for smaller diameter disks, and for longer wavelengths it is more pronounced for larger diameter disks. We can also see that there is a reduced enhancement close to the J-aggregate exciton peak. Figure 5b–f shows the emission enhancements for five specific different arrays, compared with the transmission spectra of the polaritons, $(1 - T_{norm}$ was plotted, where T_{norm} is the transmission spectra of the nanodisk arrays, normalized to the transmission of the TDBC J-aggregate layer). The emission measurements were performed after cleaning the sample with water and applying oxygen plasma, followed by spin coating with a fresh TDBC–water solution. This procedure modified the polariton resonances and reduced the Rabi splitting to $\hbar\Omega_R$ = 0.25 eV. The spectral transmission of the treated sample is shown in Supporting Figure S2, and the dips are also marked in Figure 5a as white dots. From Figures 5b–f, it can be seen that the amplitudes of the two emission lobes are correlated with the amplitudes of the transmission dips of the upper and lower polaritons, such that a redshift of the lower polariton resonance distorts the spectral shape of the emission enhancement of the lower energy lobe toward the lower frequencies. In addition, we observe that the emission is enhanced when the excitation wavelength is within the upper polariton resonance (see Supporting Figure S2). We believe that these features originate from different mechanisms. The enhancement of emission due to resonant pumping in the upper polariton branch is a consequence of the confinement of light by the nanoantennas, which leads to increased absorption and a more efficient generation of excitons. The correlation between the enhanced amplitudes of the emission lobes and the resonance of the polaritons, as well as the observed broadening, originates from enhanced emission due to an increase in the local density of states attributed to X-LSP coupled modes.

Conclusions. Most studies of the strong coupling between LSPs of metallic nanoparticles and excitons until now have used silver or gold as the plasmonic material. Here we find that aluminum plasmonic nanostructures provide an excellent platform for the generation of hybrid X-LSPs states. We measured a giant Rabi splitting of 0.4 eV, which is among the highest splitting energies reported in literature for a nanoparticle-based plasmonic system. The splitting energy is ∼20% of the uncoupled exciton transition energy and corresponds to an ultrafast energy transfer between the modes on a 10fs time scale. In addition we found that the X-LSP hybrid states can be polarized by geometrical means and that the physical parameter that limits the coupling strength is the ratio between the overlap volume V_X and total mode volume V rather than just the mode volume. Finally, we were also able to observe the effects of X-LSPs on the emission. This is an important step toward unveiling the intriguing dynamics of strongly coupled X-LSP states in plasmonic systems for which there is less evidence than has been demonstrated in recent years for exciton–polaritons in optical microcavities.[5,6,16,59] The emission measurements show enhancement correlated with the X-LSP energies due to improved resonant pumping and an increase of the density of states at the polariton energies. In light of the emerging technological applications based on strongly coupled light-matter states, the results reported in this Letter open new possibilities for using nanoscale, technologically compatible, integrated platforms based on Al, that can be adapted to work all over the visible region down to ultraviolet frequencies.

Methods. An indium tin oxide-coated glass substrate was cleaned and then spin-coated with poly(methyl methacrylate) (PMMA), followed by baking at 180 °C on a hot plate for 1 min. The nanodisk and nanorod arrays were written by an electron-beam lithography system (Raith 150) at 10 kV, followed by evaporating 40 nm of Al at 2 Å/s. The resist was then lifted off using acetone. The samples were spin-coated with a solution of 2 g of deionized water mixed with 0.015 g of cyanine dye molecules (TDBC) at 3000 rpm and sonicated for 10 min. TDBC (5,6-dichloro-2-[[5,6-dichloro-1-ethyl-3-(4-sulfobutyl)-benzimidazol-2-ylidene]-propenyl]-1-ethyl-3-(4-sulfobutyl)-benzimidazolium hydroxide, inner salt, sodium salt) was purchased from Few Chemicals. The dimensions of the nanodisks and nanorods were determined using a scanning electron microscope (SEM JSM-6700).

All measurements were performed at room temperature. Spectral transmission measurements were performed using a Xenon arc lamp, Mitutoyo 50×/0.42 objective and a fiber optic coupled spectrometer (Avantes AvaSpec-3648). The sample was placed on a nanopositioning stage (Thorlabs, NanoMax 606) which was controlled by a computer. Emission measurements were recorded using a Zeiss axio observer Z1m microscope in reflection mode. The excitation source was a tunable femtosecond laser (Chameleon OPO VIS, pulse width of 140 fs, repetition rate of 80 MHz). Emissions were collected by a spectrometer (Andor, Shamrock 303i) with a 100×/0.75 objective.

Three dimensional finite difference time domain (FDTD) simulations were performed using Lumerical Solutions software. The simulations were periodic in the x–y plane with Γ = 180 nm for the nanodisk arrays and with Γ_y = 150 nm and Γ_x = 200 nm for the nanorod arrays. The simulated structures comprised a glass substrate, modeled as a dielectric with refractive index of n = 1.51 coated with a 30 nm layer of indium tin oxide (ITO) modeled using data from the Sopra Material Database. The 40 nm high nanodisks or nanorods on top of this substrate were modeled using Palik data for Al.[60] The TDBC coating was modeled as a 20 nm layer of a single Lorentzian oscillator $\epsilon_{Lorentz(\omega)} = \epsilon_\infty + (f\omega_X^2/(\omega_X^2 - \omega^2 - i\gamma_X\omega))$, where ϵ_∞ = 2.56 comes from the bound electron permittivity, ω_X = 3.22 × 10^{15} [rad/s] is the oscillator frequency, γ_X = 2.45 × 10^{13} [rad/s] is the damping constant, and f = 0.45 is the oscillator strength. The shape of the nanorods was modeled as an ellipse with a constant minor axis length of 25 nm.

■ ASSOCIATED CONTENT

Supporting Information

The Supporting Information is available free of charge on the ACS Publications website at DOI: 10.1021/acs.nanolett.5b02584.

S1: Nanorod array simulations, FDTD simulations of bare and covered nanorod arrays, calculations for exciton and LSP fractions of the upper or lower X-LSP polariton states of the nanorod arrays. S2: Emission enhancement of TDBC J-aggregate coated nanodisk arrays for excitation at different wavelengths. S3: Estimation of the number of excitons in the mode volume (PDF)

DOI: 10.1021/acs.nanolett.5b02584
Nano Lett. 2015, 15, 6215–6221

AUTHOR INFORMATION

Corresponding Author

*E-mail: eladeiz@post.tau.ac.il.

Notes

The authors declare no competing financial interest.

ACKNOWLEDGMENTS

This work was supported by the Israeli Science Foundation, Grant No. 1331/13 and by the European Commission Marie Curie Career Integration Grant No. 333821.

REFERENCES

(1) Goy, P.; Raimond, J. M.; Gross, M.; Haroche, S. *Phys. Rev. Lett.* **1983**, *50*, 1903−1906.
(2) Deng, H.; Haug, H.; Yamamoto, Y. *Rev. Mod. Phys.* **2010**, *82*, 1489−1537.
(3) Törmä, P.; Barnes, W. L. *Rep. Prog. Phys.* **2015**, *78*, 13901.
(4) Tassone, F.; Yamamoto, Y. *Phys. Rev. B: Condens. Matter Mater. Phys.* **1999**, *59*, 10830−10842.
(5) Daskalakis, K. S.; Maier, S. A.; Murray, R.; Kéna-Cohen, S. *Nat. Mater.* **2014**, *13*, 271−278.
(6) Plumhof, J. D.; Stöferle, T.; Mai, L.; Scherf, U.; Mahrt, R. F. *Nat. Mater.* **2014**, *13*, 247−252.
(7) Saba, M.; Ciuti, C.; Bloch, J.; Thierry-Mieg, V.; André, R.; Dang; le, S.; Kundermann, S.; Mura, A.; Bongiovanni, G.; Staehli, J. L.; et al. *Nature* **2001**, *414*, 731−735.
(8) Vasa, P.; Pomraenke, R.; Cirmi, G.; De Re, E.; Wang, W.; Schwieger, S.; Leipold, D.; Runge, E.; Cerullo, G.; Lienau, C. *ACS Nano* **2010**, *4*, 7559−7565.
(9) Vasa, P.; Wang, W.; Pomraenke, R.; Lammers, M.; Maiuri, M.; Manzoni, C.; Cerullo, G.; Lienau, C. *Nat. Photonics* **2013**, *7*, 128−132.
(10) Hutchison, J. A.; Schwartz, T.; Genet, C.; Devaux, E.; Ebbesen, T. W. *Angew. Chem., Int. Ed.* **2012**, *51*, 1592−1596.
(11) Coles, D. M.; Yang, Y.; Wang, Y.; Grant, R. T.; Taylor, R. A.; Saikin, S. K.; Aspuru-Guzik, A.; Lidzey, D. G.; Tang, J. K.-H.; Smith, J. M. *Nat. Commun.* **2014**, *5*, 5561.
(12) Carmeli, I.; Cohen, M.; Heifler, O.; Lilach, Y.; Zalevsky, Z.; Mujica, V.; Richter, S. *Nat. Commun.* **2015**, *6*, 7334.
(13) Manjavacas, A.; Abajo, F. J. G.; Nordlander, P. *Nano Lett.* **2011**, *11*, 2318−2323.
(14) Weisbuch, C.; Nishioka, M.; Ishikawa, A.; Arakawa, Y. *Phys. Rev. Lett.* **1992**, *69*, 3314−3317.
(15) Skolnick, M. S.; Fisher, T. A.; Whittaker, D. M. *Semicond. Sci. Technol.* **1998**, *13*, 645−669.
(16) Lidzey, D. G.; Bradley, D. D. C.; Virgili, T.; Armitage, A.; Skolnick, M. S.; Walker, S. *Phys. Rev. Lett.* **1999**, *82*, 3316−3319.
(17) Ellenbogen, T.; Steinvurzel, P.; Crozier, K. B. *Appl. Phys. Lett.* **2011**, *98*, 261103.
(18) Van Vugt, L. K.; Rühle, S.; Ravindran, P.; Gerritsen, H. C.; Kuipers, L.; Vanmaekelbergh, D. *Phys. Rev. Lett.* **2006**, *97*, 147401.
(19) Ellenbogen, T.; Crozier, K. B. *Phys. Rev. B: Condens. Matter Mater. Phys.* **2011**, *84*, 161304.
(20) Katsuyama, T.; Ogawa, K. *J. Appl. Phys.* **1994**, *75*, 7607.
(21) Takazawa, K.; Inoue, J.; Mitsuishi, K.; Takamasu, T. *Phys. Rev. Lett.* **2010**, *105*, 067401.
(22) Väkeväinen, A. I.; Moerland, R. J.; Rekola, H. T.; Eskelinen, A.-P.; Martikainen, J.-P.; Kim, D.-H.; Törmä, P. *Nano Lett.* **2014**, *14*, 1721−1727.
(23) Rodriguez, S. R. K.; Feist, J.; Verschuuren, M. A.; Garcia Vidal, F. J.; Gómez Rivas, J. *Phys. Rev. Lett.* **2013**, *111*, 166802.
(24) Bellessa, J.; Bonnand, C.; Plenet, J.; Mugnier, J. *Phys. Rev. Lett.* **2004**, *93*, 036404.
(25) Hakala, T.; Toppari, J.; Kuzyk, A.; Pettersson, M.; Tikkanen, H.; Kunttu, H.; Törmä, P. *Phys. Rev. Lett.* **2009**, *103*, 053602.
(26) Vasa, P.; Wang, W.; Pomraenke, R.; Lammers, M.; Maiuri, M.; Manzoni, C.; Cerullo, G.; Lienau, C. *Nat. Photonics* **2013**, *7*, 128−132.
(27) Eizner, E.; Ellenbogen, T. *Appl. Phys. Lett.* **2014**, *104*, 223301.
(28) Schwartz, T.; Hutchison, J. A.; Genet, C.; Ebbesen, T. W. *Phys. Rev. Lett.* **2011**, *106*, 196405.
(29) Bellessa, J.; Symonds, C.; Vynck, K.; Lemaitre, A.; Brioude, A.; Beaur, L.; Plenet, J.; Viste, P.; Felbacq, D.; Cambril, E.; et al. *Phys. Rev. B: Condens. Matter Mater. Phys.* **2009**, *80*, 033303.
(30) Zengin, G.; Johansson, G.; Johansson, P.; Antosiewicz, T. J.; Käll, M.; Shegai, T. *Sci. Rep.* **2013**, *3*, 3074.
(31) Chantharasupawong, P.; Tetard, L.; Thomas, J. *J. Phys. Chem. C* **2014**, *118*, 23954−23962.
(32) Zengin, G.; Wersäll, M.; Nilsson, S.; Antosiewicz, T. J.; Käll, M.; Shegai, T. *Phys. Rev. Lett.* **2015**, *114*, 157401.
(33) Sugawara, Y.; Kelf, T.; Baumberg, J.; Abdelsalam, M.; Bartlett, P. *Phys. Rev. Lett.* **2006**, *97*, 266808.
(34) Fofang, N. T.; Park, T.-H.; Neumann, O.; Mirin, N. A.; Nordlander, P.; Halas, N. J. *Nano Lett.* **2008**, *8*, 3481−3487.
(35) Schlather, A. E.; Large, N.; Urban, A. S.; Nordlander, P.; Halas, N. J. *Nano Lett.* **2013**, *13*, 3281−3286.
(36) Smith, D. R.; Pendry, J. B.; Wiltshire, M. C. K. *Science* **2004**, *305*, 788−792.
(37) Kildishev, A. V.; Boltasseva, A.; Shalaev, V. M. *Science* **2013**, *339*, 1232009.
(38) Yu, N.; Capasso, F. *Nat. Mater.* **2014**, *13*, 139−150.
(39) Segal, N.; Keren-Zur, S.; Hendler, N.; Ellenbogen, T. *Nat. Photonics* **2015**, *9*, 180−184.
(40) Avayu, O.; Eisenbach, O.; Ditcovski, R.; Ellenbogen, T. *Opt. Lett.* **2014**, *39*, 3892−3895.
(41) Eisenbach, O.; Avayu, O.; Ditcovski, R.; Ellenbogen, T. *Opt. Express* **2015**, *23*, 3928−3936.
(42) Langhammer, C.; Schwind, M.; Kasemo, B.; Zoric, I. *Nano Lett.* **2008**, *8*, 1461−1471.
(43) Knight, M. W.; Liu, L.; Wang, Y.; Brown, L.; Mukherjee, S.; King, N. S.; Everitt, H. O.; Nordlander, P.; Halas, N. J. *Nano Lett.* **2012**, *12*, 6000−6004.
(44) Knight, M. W.; King, N. S.; Liu, L.; Everitt, H. O.; Nordlander, P.; Halas, N. J. *ACS Nano* **2013**, *8*, 834−840.
(45) Ellenbogen, T.; Seo, K.; Crozier, K. B. *Nano Lett.* **2012**, *12*, 1026−1031.
(46) Olson, J.; Manjavacas, A.; Liu, L.; Chang, W.-S.; Foerster, B.; King, N. S.; Knight, M. W.; Nordlander, P.; Halas, N. J.; Link, S. *Proc. Natl. Acad. Sci. U. S. A.* **2014**, *111*, 14348−14353.
(47) McClain, M. J.; Schlather, A.; Ringe, E.; King, N. S.; Liu, L.; Manjavacas, A.; Knight, M.; Kumar, I.; Whitmire, K. H.; Everitt, H. O.; et al. *Nano Lett.* **2015**, *15*, 2751−2755.
(48) Lawrie, B. J.; Kim, K.-W.; Norton, D. P.; Haglund, R. F., Jr *Nano Lett.* **2012**, *12*, 6152−6157.
(49) Dicke, R. H. *Phys. Rev.* **1954**, *93*, 99−110.
(50) Garraway, B. M. *Philos. Trans. R. Soc., A* **2011**, *369*, 1137−1155.
(51) Liu, X.; Galfsky, T.; Sun, Z.; Xia, F.; Lin, E.; Lee, Y.-H.; Kéna-Cohen, S.; Menon, V. M. *Nat. Photonics* **2014**, *9*, 30−34.
(52) Savasta, S.; Saija, R.; Ridolfo, A.; Di Stefano, O.; Denti, P.; Borghese, F. Plexitonic Nanoparticle. *ACS Nano* **2010**, *4*, 6369−6376.
(53) Khitrova, G.; Gibbs, H. M.; Kira, M.; Koch, S. W.; Scherer, A. *Nat. Phys.* **2006**, *2*, 81−90.
(54) Antosiewicz, T. J.; Apell, S. P.; Shegai, T. *ACS Photonics* **2014**, *1*, 454−463.
(55) Gunnarsson, L.; Rindzevicius, T.; Prikulis, J.; Kasemo, B.; Käll, M.; Zou, S.; Schatz, G. C. *J. Phys. Chem. B* **2005**, *109*, 1079−1087.
(56) Saikin, S. K.; Eisfeld, A.; Valleau, S.; Aspuru-Guzik, A. *Nanophotonics* **2013**, *2*, 21−38.
(57) Khurgin, J. B.; Sun, G. *J. Opt. Soc. Am. B* **2009**, *26*, B83−B95.
(58) Khurgin, J. B. *Nat. Nanotechnol.* **2015**, *10*, 2−6.
(59) Kéna-Cohen, S.; Forrest, S. R. *Nat. Photonics* **2010**, *4*, 371−375.
(60) Palik, E. D. *Handbook of Optical Constants of Solids*; Academic Press: New York, 1998; Vol. 3.

DOI: 10.1021/acs.nanolett.5b02584
Nano Lett. 2015, 15, 6215−6221